Probabilistic extraction of deep sulcal landmarks from cortical surfaces

****

*****
*****
*****
*****
*****
*****

Abstract. We introduce a probabilistic method to extract deep sulcal landmarks from human MRI cortical surfaces. This method overcomes difficulties associated with hard thresholds and rules used by existing methods. Each point on the surface assumes a likelihood value based on its local depth and Gaussian curvature, and adaptive functions take subject variability into account. A hidden Markov measure field model suppresses weaker pit candidates in the vicinity of stronger ones. The method provides a stable set of landmarks that correspond well with manually delineated boundaries.

Keywords: sulcal pits, sulcal landmarks, Bayes, Markov field

1 Introduction

In the folds of the human cerebral cortex, the deepest local regions are believed to correspond to the first cortical folds that form during early development [1, 2]. These deep sulcal landmarks, or sulcal *pits*, may offer stable anatomical landmarks [1, 3], and as such could not only increase our understanding of brain development but also provide corresponding landmarks across brains. Previous studies presenting sulcal pit extraction methods have shown interesting clusters in their distributions [1, 4]. Recently, an analysis of sulcal pits was used to show a correspondence between sulcal pit locations and intelligence [5].

Even with an increasing appreciation of the significance of sulcal pits, the methods used to extract them have not been thoroughly studied. The pit extraction methods used in previous studies use hard thresholds and rules that impact subsequent analysis in limiting and possibly inappropriate ways. When selecting the set of final pits from the clusters of candidate points, such rigid formulations make simplifying assumptions that do not account for the complicated relationships among the points. These assumptions can lead to arbitrary decisions about which points are considered pits. Moreover, hard thresholds do not consider anatomical variability across individuals.

In this study we formulate a probabilistic approach to pit extraction. Based on local geometric properties, each point assumes a continuous valued *likelihood*, which expresses the certainty that the point should be considered a pit. An adaptive model estimates the likelihood to account for inter-individual variability. To obtain the final set of sulcal pits, a hidden Markov measure field (HMMF) model [6] suppresses the less likely pit candidates in the vicinity of stronger ones. The degree of influence each point has on other candidates depends on its likelihood value and distance to other candidates.

Section 2 presents the probabilistic model and introduces the data and software used in the experiments. Section 3 presents the results of the experiments, followed by a concluding discussion in Section 4.

2 Methods

2.1 General pit extraction framework

This formulation is a simplified, two-class version of the HMMF model. The current implementation differs from prior work primarily in the Markov field cliques and potential functions (see Section 2.2). Let the input surface mesh be S, the surface domain Ω and $r \in \Omega$ be points (vertices) on the surface. The pit extraction task can be formulated as finding the label field f that maximizes the posterior probability $P(f|S)$. The label field accepts two values, $f(r) = 1$ if the point is considered a pit, and $f(r) = 2$ otherwise. The label field f is computed through a continuous valued vector field q that maximizes the posterior probability $P(q|S)$. Each vertex r is associated with a two-dimensional vector $q(r) = \big[q_1(r)\ q_2(r)\big]$, constrained by $q_1(r) + q_2(r) = 1$ and $q_1, q_2 \geq 0$. The values $f(r)$ are considered as independent samples from $q(r)$, with $P(f|q) = \prod_{r\in\Omega} q_{f(r)}(r)$, where $q_{f(r)}(r)$ is the component of $q(r)$ corresponding to $f(r)$.

The posterior distribution $P(q|S)$ is obtained from the Bayes rule

$$P(q|S) = \frac{1}{R} P(S|q)P(q), \tag{1}$$

where R is a positive normalizing term. $P(S|q)$ is defined as (see [6]):

$$P(S|q) = \prod_{r\in\Omega} \sum_{k=1}^{2} P(S(r)|f(r) = k) q_k(r). \tag{2}$$

To simplify notation, we denote $P(S(r)|f(r) = k) = L_k(S(r))$ in the following. The prior distribution $P(q)$ is prescribed as a Markov field

$$P(q) = \frac{1}{J} \exp\left[-\sum_{C} W_C(q)\right], \tag{3}$$

where J is a positive constant, C are neighborhood cliques, and W_C are potential functions used to control the influence that points in a clique have on each other.

By merging (1), (2), and (3): $P(q|S) = (JR)^{-1} \exp[-U(q)]$, where

$$U(q) = -\sum_{r\in\Omega} \log\left[\sum_{k=1}^{2} L_k(S(r))q_k(r)\right] + \sum_{C} W_C(q). \quad (4)$$

Since $(JR)^{-1} > 0$, the MAP estimator $q^* = \arg\max_q P(q|S)$ can be found by minimizing $U(q)$. Then the optimal estimator f^* is obtained by assigning $f^*(r) = 1$ if $q_1^*(r) > q_2^*(r)$, and $f^*(r) = 2$ otherwise. For the formulation to be complete, we need to define the terms in (4), which is the topic of Section 2.2.

2.2 Likelihood functions and field potentials

For defining the likelihood functions in (4), we consider qualities that make a surface point a likely pit. For example, previous work based on watershed segmentation [4] defined parameters to specify minimum values for basin size, depth, and pairwise distance and ridge height between pits. In our approach, local surface characteristics define a continuous valued likelihood for each point without using thresholds. To provide easy interpretation of the model, we use only two variables, namely cortical depth and local Gaussian curvature. High depth and high Gaussian curvature (with positive mean curvature) correspond to high likelihood values.

Let $D(r)$ and $K(r)$ be the respective local cortical depth and Gaussian curvature at r. Due to the lack of ground truth training data, we use an empirical model to derive our likelihood functions. The model assumes measures D and K to be independent variables associated with sigmoidal likelihoods that are mapped between 0 and 1: $L_1(S(r)) = F_1(D(r))F_1(K(r))$, and

$$F_1(\{D,K\}(r)) = \frac{1}{1+\exp[-\alpha_{D,K}(\{D,K\}(r) - \beta_{D,K})]}. \quad (5)$$

The parameter $\alpha_{D,K}$ controls the slope of the function and $\beta_{D,K}$ is the value in $\{D,K\}(r)$ that is mapped to 0.5.

To make the model adaptive to inter-individual variability, parameter values are estimated from the data, separately for each cortical surface. This ensures that the model is independent of the methods used to measure depth and curvature. We set the parameters so that most of the smaller depth and curvature values have likelihoods close to zero, and to provide large contrast for the highest values of depth and curvature. For the experiments below, β_D was the 85^{th} percentile of all depth values on the surface. With β_D fixed, α_D was found so that the 95^{th} percentile of depth values was 0.80. $\beta_K = 0$ was fixed and α_K was found so that the 85^{th} percentile of curvature values was 0.90. Fig. 1 shows an example of the resulting likelihood function. The likelihood for $f(r) = 2$ is the complement: $L_2(S(r)) = 1 - L_1(S(r))$.

As in previous work [1, 4], we define pit candidates as local maxima of depth, which also ensures that the candidates have positive mean curvature. The vertex density varied significantly in different parts of the cortical surface mesh, with

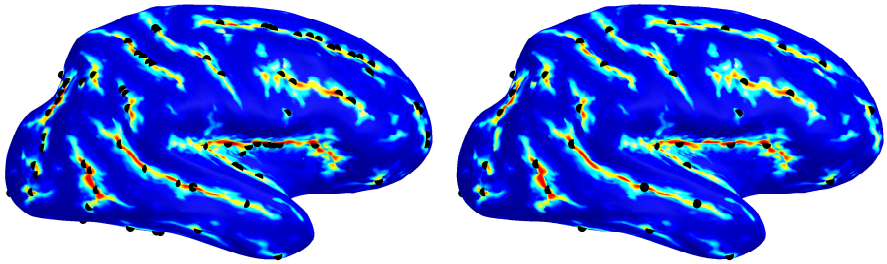

(a) (b)

Fig. 1. Pit extraction example on an inflated cortical surface (Markov field weight $\lambda = 3$, see Eq. (6)), color represents likelihood values (see colorbar in Fig. 2) and black markers correspond to locations of (a) pit candidates with likelihood values larger than 0.5, and (b) extracted pits.

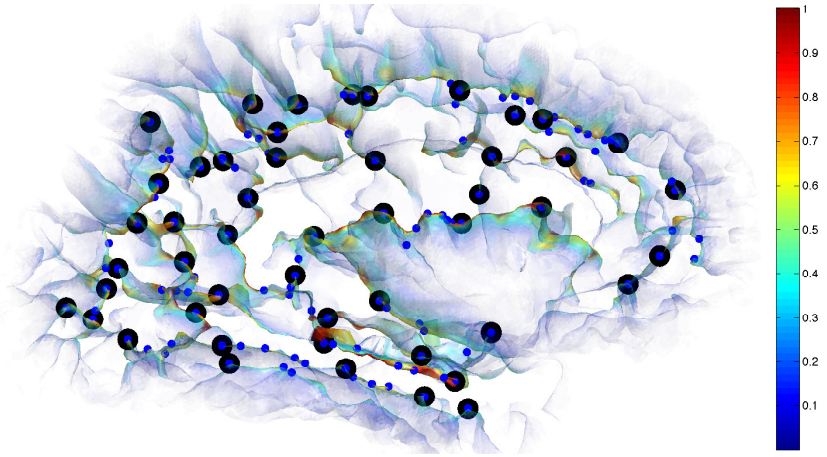

Fig. 2. Pit extraction example on a semi-transparent uninflated cortical surface (Markov field weight $\lambda = 3$, see Eq. (6), same subject as in Fig. 1). Color indicates likelihood value, and transparency increases with decreasing likelihood to visually enhance areas of high likelihood. Blue circles represent pit candidates with likelihood values larger than 0.5 and black circles represent extracted pits.

the mean edge length and standard deviation being 1.0 ± 0.43 mm. To make the density of local maxima independent of the sampling of the surface, we define local maxima of depth as the deepest points within a radius of 1.5 mm geodesic distance [7], which was longer than 89% of edge lengths.

Considering solely likelihood values for extraction results in a high number of pits that are often located close together (see Fig. 1a). In contrast to thresholds used in previous work [1, 4], here the Markov field potential function penalizes the extraction of pits located close together. To extract the strongest pit points and suppress the weaker candidates, we use pairwise cliques C, so that all the other points on the surface are considered. The potential between two points r_1

and r_2 is then

$$W_{r_1 r_2} = \lambda \exp\left[\frac{-d_g(r_1, r_2)^2}{2\sigma^2}\right] q_1(r_1) q_1(r_2), \tag{6}$$

where d_g is the geodesic distance between the points, σ controls how fast the potential decreases with distance, and λ is a scalar weight for adjusting the balance between the likelihood term and the Markov field term. We set $\sigma^2 = 75$ so that pairwise distances of the resulting pits are similar to those in previous work [1, 4] for a range of values of λ. We evaluated the model for different values of λ in Section 3. Figs. 1b, 2 show an example of the resulting pit extraction.

2.3 Data and Software

We conducted our experiments on 20 T1-weighted brain MRI volumes of healthy volunteers from the publicly available "Multi-Modal MRI Reproducibility Resource" [8]. We used FreeSurfer [9, 10] to extract the outer cortical surfaces from each image and to compute a convexity map for each surface, which we used as a measure of surface depth. We used publicly available toolboxes to compute all geodesic distances [7, 11] and Gaussian curvatures [12]. Curvature computation failed for one of the 21 subjects, so we removed this subject from the study. For evaluation, we used manually edited anatomical labels of the brains provided by **REMOVED** according to a new cortical surface labeling protocol by **REMOVED** based on a simplified version of the Desikan-Killiany protocol [13] that relies to a greater degree on robust sulcal landmarks. The labeling was done with no regard to pit locations or knowledge that the labeled data would be used for a pit extraction study.

3 Results

3.1 Distribution of pits

To analyze the stability of the method, we examined the number of extracted pits and the minimum distance between any two pits for different values of λ, for both hemispheres of each of the 20 brains. Table 1 shows the results.

With values of λ between 2.0 and 5.0, the extraction resulted in a stable set of points, with the standard deviation in the number of extracted pits in one hemisphere varying between 4.1 and 4.6. With these values, the mean number of extracted pits declined steadily from 45.6 to 40.6, and the mean minimum distance between any two pits increased from 15.6 mm to 19.4 mm.

When ignoring the Markov field effect ($\lambda = 0$), the extracted pits were simply all points with likelihood greater than 0.5. This resulted in a very high number of extracted points, 118.2 per hemisphere on average. The extracted points were often located close to each other, with a mean minimum distance of 1.6 mm. Increasing the value of λ to 1.0 caused the Markov field to suppress a large number of points, but some strong pit candidates still remained in close proximity to one another, as indicated by the smallest minimum distance of 1.9 mm.

Table 1. Number of extracted pits and minimum distance between any two pits in a hemisphere, averaged across 20 subjects (40 hemispheres), for different values of λ

	Number of pits				Minimum distance (mm)			
λ	Mean	SD	Min	Max	Mean	SD	Min	Max
0.0	118.2	15.3	85	149	1.6	0.1	1.5	1.8
1.0	52.2	5.1	41	61	8.5	3.5	1.9	13.4
2.0	45.6	4.2	35	52	15.6	1.8	12.0	19.8
3.0	43.3	4.6	31	50	17.4	2.0	12.0	21.4
4.0	41.5	4.1	31	48	18.6	1.2	16.4	21.4
5.0	40.6	4.1	30	47	19.4	1.4	15.5	22.8

The absolute mean difference in the number of extracted pits between the two hemispheres of each subject was 2.55 and the maximum difference was 8 pits (for $\lambda = 3$). For 15 of the 20 subjects the difference was 3 pits or fewer. This demonstrates that the difference in the number of extracted pits between the two hemispheres is small on average.

3.2 Pit locations with respect to manual labels

We compared the locations of the extracted pits to the boundaries of manually defined labels (every vertex is assigned a label), by computing the geodesic distance between the pit vertex and the label boundary. The distance of a vertex to the boundary was defined as 0 if any of the neighboring vertices had a different label. The value $\lambda = 3.0$ was chosen for these experiments, but we expect the method to produce similar results for other values between 2.0 and 5.0, as the method was shown to be robust with respect to this variable. Fig. 3 shows two examples of manual labels and extracted pits.

Of the total of 1733 pits extracted from the 40 hemispheres, 47% were located less than 1 mm from a label boundary, and 73% were less than 3 mm from a boundary. The median distance of a pit from a label boundary was 1.1 mm.

A high number (267) of pits were also located within 3 mm of junctions of three manual labels. Despite the infrequency of these junctions on the manually labeled cortical surface, these junction pits comprise 15% of the total number of pits. The specific junction that had the most pits across all subjects was at the intersection of the caudal middle frontal, precentral, and superior frontal gyri. A pit occurred within 3 mm of this location in 23 out of the 40 hemispheres. The location is highlighted in Fig. 3.

Finally, we identified five major sulci for each of the 40 hemispheres by the manual label boundaries that run through them, and recorded the number of pits that occurred within 3 mm of each of these sulci. The results averaged across 40 hemispheres in 20 subjects were (sulcus name, mean $\pm$ standard deviation): (1) Superior frontal: 3.3 ± 1.2, (2) Precentral: 2.4 ± 1.1, (3) Postcentral: 2.1 ± 0.6, (4) Intraparietal: 2.1 ± 0.8, (5) Cingulate: 3.4 ± 1.3. The mean number of pits varied between 2.1 and 3.4 for each of the five sulci. The standard deviation of

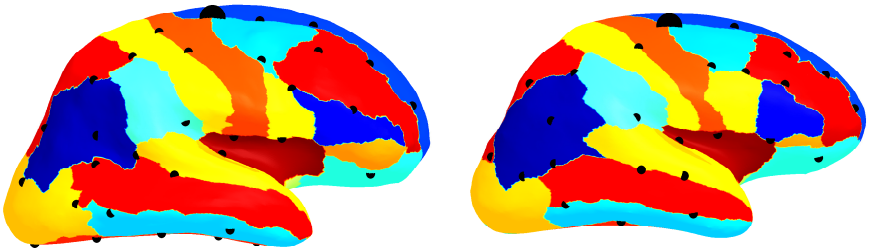

(a) (b)

Fig. 3. The inflated right hemisphere of two subjects with manual labels (colors) and extracted pits (black markers). The large marker at the top of each brain is located at the junction of three labels where a pit was found for more than half of the subjects.

the number of pits was relatively low, between 0.6 and 1.3. However, there were cases where no pits or only one pit was found close to the sulcus. This may be partly due to the chosen threshold value.

4 Discussion

We introduced a probabilistic method to extract deep sulcal landmarks to improve on existing approaches that rely on hard thresholds and rules. The resulting points were shown to be stable and they correspond well to manually delineated boundaries. Since our method is reliable without being rigid, it enables a more robust analysis of sulcal pits in future studies. We intend to refine the model further as we study the properties of these pits in a larger sample of labeled brain images.

The lack of ground truth data prompted the use of an empirical likelihood function. In comparison to other approaches, our likelihood function generates values that change gradually without using hard thresholds. Our approach uses only two variables, cortical depth and Gaussian curvature. Adding new variables could provide better extraction results, even though it would also complicate function design. The Markov field model uses the likelihood values and discourages spatially clustered configurations of pits. The influence of the Markov field depends on the pairwise geodesic distances between pits, and the model was tuned to produce pit distances that were in line with previous work [1, 4].

It is not clear from our study whether the variation in the number of extracted pits across subjects was due to anatomical variation across individuals or to the extraction method. The difference in the number of pits between hemispheres was very small on average, which implies that larger variability in the number of pits across subjects is not random. Even though our likelihood model is adaptive so as to account for anatomical variation, the Markov field effect depends on a fixed distance-based weight, which might have decreased the number of pits for smaller brains. In future work, we aim to make the distance function weight dependent on brain size.

Extracted pits that are very close to manually labeled boundaries motivate the use of pits in landmark-driven, registration-based labeling. Automated identification of individual pits would help establish stable points across individuals. Since recent findings based on the analysis of sulcal pits have provided intriguing results, further studies of sulcal pits promises to reveal other applications, such as longitudinal analysis of morphology, and possibly biomarkers for diagnosis of or prediction of treatment response in neuropsychiatric illnesses.

Acknowledgements

******
******

References

1. Lohmann, G., Von Cramon, D.Y., Colchester, A.C.F.: Deep Sulcal Landmarks Provide an Organizing Framework for Human Cortical Folding. Cerebral Cortex, vol. 18 (2008)
2. Régis, J., Mangin, J.F., Ochiai, T. Frouin, V., Riviére, D., Cachia, A., Tamura, M., Samson, Y.: "Sulcal root" generic model: A hypothesis to overcome the variability of the human cortex folding patterns. Neurologia medico-chirurgica, vol. 45 (2005)
3. Clouchoux, C., Coulon, O., Anton, J.L., Mangin, J.F., Régis, J.: A new cortical surface parcellation model and its automatic implementation. MICCAI (2006)
4. Im, K., Jo, H.J., Mangin, J.F., Evans, A.C., Kim, S.I., Lee, J.M.: Spatial Distribution of Deep Sulcal Landmarks and Hemispherical Asymmetry on the Cortical Surface. Cerebral Cortex, vol. 20 (2010)
5. Im, K., Choi, Y.Y., Yang, J.J., Lee, K.H., Kim, S.I., Grant, P.E., Lee, J.M.: The relationship between the presence of sulcal pits and intelligence in human brains. NeuroImage, vol. 55 (2011)
6. Marroquin, J.L., Santana, E.A., Botello, S.: Hidden Markov measure field models for image segmentation. IEEE Transactions on Pattern Analysis and Machine Intelligence, vol. 25 (2003)
7. Mitchell, J.S.B., Mount, D.M., Papadimitriou, C.H.: The Discrete Geodesic Problem. SIAM Journal on Computing, vol. 16 (1987)
8. Landman, B.A., Huang, A.J., Gifford, A., Vikram, D.S., Lim, I.A.L., Farrell, J.A.D., Bogovic, J.A., Hua, J., Chen, M., Jarso, S., et al.: Multi-Parametric Neuroimaging Reproducibility: A 3T Resource Study. NeuroImage, vol. 54 (2010)
9. Dale, A.M., Fischl, B., Sereno, M.I.: Cortical Surface-Based Analysis: I. Segmentation and Surface Reconstruction. NeuroImage, vol. 9 (1999)
10. Fischl, B., Sereno, M.I., Dale, A.M.: Cortical Surface-Based Analysis: II: Inflation, Flattening, and a Surface-Based Coordinate System. NeuroImage, vol. 9 (1999)
11. Kirsanov, D.: Exact geodesic for triangular meshes (http://www.mathworks.com/matlabcentral/fileexchange/18168). MATLAB Central File Exchange (2007). Retrieved February 13, 2012.
12. Peyre, G.: Toolbox Graph (http://www.mathworks.com/matlabcentral/fileexchange/5355). MATLAB Central File Exchange (2004). Retrieved February 15, 2012.
13. Desikan, R.S., Segonne, F., Fischl, B., Quinn, B.T., Dickerson, B.C., Blacker, D., et al.: An automated labeling system for subdividing the human cerebral cortex on MRI scans into gyral based regions of interest. NeuroImage, vol. 31 (2006)